

MATERIAL CHARACTERIZATION FOR LIGHTWEIGHT THIN WALL STRUCTURES USING
LASER POWDER BED FUSION ADDITIVE MANUFACTURING

Sean Dobson*, Yan Wu†, Li Yang†

*Department of Mechanical Engineering, University of Louisville, Louisville, KY 40292

†Department of Industrial Engineering, University of Louisville, Louisville, KY 40292

Abstract

In this study the geometry-process-material characteristics of the Ti6Al4V thin wall features fabricated by the EOS M270 laser melting powder bed fusion (LM-PBF) additive manufacturing (AM) was investigated. Samples with varying wall thickness, orientation, scanning speeds and laser power were fabricated and analyzed. The dimensional accuracies, microstructural characteristics and mechanical properties of the samples were evaluated experimentally. The results clearly indicated the significant coupling effects between the geometry design of these thin wall features and their material properties, which is critical to the design and manufacturing of many AM lightweight structures. By identifying significant design and process parameters for the thin wall structures, this study will enable further investigations of the integrated design theories for the AM lightweight structures.

1. Introduction

The use of cellular structures for engineering applications has been subjected to extensive research in recent decades [1-10]. These structures are highly attractive for an extremely broad range of applications from aerospace, automobile and defense to energy and biomedicine. Cellular structures exhibit a range of exceptional characteristics including high mechanical properties-to-weight ratios (e.g. elastic modulus, bending strength, shear modulus, shear strength, energy absorption, indentation resistance) [11-13], unique thermal and fluid flow properties that can be tailor-controlled [14-16], and large surface area-to-volume ratios [17, 18]. With the combinational design of both base materials and the geometries, unique functionality can be potentially achieved for cellular structures to be used for more efficient design integrations. Examples that demonstrate the potentials of cellular structure based designs are shown in Figure 1. Figure 1a shows the redesign of an aircraft engine bracket, which achieved 80% weight reduction with no loss of yield strength [19]. Figure 1b shows an integrated lightweight design of a hydraulic intake manifold for the V-22 Osprey aircraft, which also achieved an impressive 70% weight reduction with improved fluid flow performance [20, 21].



a. Engine bracket design optimization [19]

b. Hydraulic intake manifold [20]

Figure 1 Lightweight cellular designs in aerospace and Naval applications

Various design theories have been developed for the design and optimization of lightweight structures. These design tools, which largely fall into two categories, namely cellular structure designs and topology optimization designs, generally define the design problems using base materials with known properties. Due to the complexity of the geometries, these lightweight designs are largely infeasible for traditional manufacturing technologies, which makes additive manufacturing (AM) the only practical option. However, the unique process characteristics of AM also impose challenges to the design of lightweight structures, particularly in the representation of material properties.

Generally AM materials exhibit anisotropy due to the layer-wise based process. For powder bed fusion AM (PBF-AM), which has been extensively used in the direct manufacturing of metal structures, there are also additional factors that contribute to the material property heterogeneity, such as the choice of scanning strategies, the amount of input energy and the use of powder feedstock that exhibits intrinsic size stochasticity. As a result, the properties of PBF-AM-fabricated materials exhibit more complex anisotropic characteristics as well as more significant variability. For the fabrication of lightweight designs with small feature dimensions, it could be expected that such process-induced property and quality issues are even more signified. However, relatively little studies have been carried out to thoroughly investigate these unique “materials”. Therefore, the aim of this study was to initiate the efforts of establishing a more comprehensive understanding of the material properties of PBF-AM lightweight features. In this study, various geometry factors including the build orientation and dimensions of the features, as well as identify key process parameters, were investigated for their effects on the dimensional accuracy, defect and mechanical properties of the Ti6Al4V thin-wall features fabricated via laser melting PBF (LM-PBF). The results were intended to not only provide preliminary database for these materials but also help establishing knowledge about the critical design factors for successful fabrication of these structures.

2. Experimental Approach

In this study, the thin wall samples as shown in Figure 2 and Figure 3. The thin wall features extend out from bases that are also part of the structures, so that during the fabrication process the effect of the build substrate is minimized. The LM-PBF system used in this study is the EOS M270. In order to investigate the potential coupling effects among the geometry and process input variables, a full-factorial experimental design was adopted for the study. Table 1 shows the input variables investigated as well as their levels. The laser power and scan speed parameters were chosen based on an earlier study with the Ti6Al4V thin strut features in order to provide additional

references for comparison in the future. The 9 combinations of process parameters are further shown in Table 2. It is noted that parameter set 3 is currently used by the EOS M270 system as the default support structure parameters, which was considered to provide a baseline for this study. 4 batches of samples were fabricated, and each batch includes 135 samples. The total number of samples fabricated for this study is 675.

Factor	Level
Laser Power (W)	60, 80, 100
Scan Speed (mm/s)	300, 400, 500
Build Orientation (°)	15, 45, 75
Scanning Strategy	Contour + Hatch
Beam Offset (μm)	40
Thickness (mm)	.1, .3, .5, .7, .9

Table 1: Sample experimental design

Parameter Set	Power (W)	Scan Speed (mm/s)	Layer Thickness (mm)	Hatch Spacing (mm)	Energy Density (J/mm ³)
1	60.00	400.00	0.03	0.01	500
2	60.00	300.00	0.03	0.01	666.6667
3	80.00	400.00	0.03	0.01	666.6667
4	100.00	500.00	0.03	0.01	666.6667
5	100.00	300.00	0.03	0.01	1111.111
6	60.00	500.00	0.03	0.01	400
7	80.00	300.00	0.03	0.01	888.8889
8	80.00	500.00	0.03	0.01	533.3333
9	100.00	400.00	0.03	0.01	833.3333

Table 2: Process parameter sets for sample fabrication

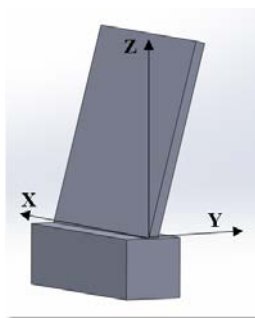


Figure 2. Optical microscopy sample design, 75°. Dimensions of (10mm X 10mm X design thickness).

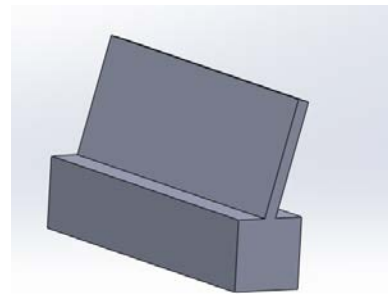


Figure 3. Three-point bending sample design, 75°. Dimensions of (15mm X 5mm X design thickness).

After fabrication, all samples were then cut using a low speed saw from their rectangular base. The wall thickness of the fabricated samples was measured by caliper and compared with the nominal design thickness for dimensional accuracy. The porosities of the samples were obtained by using optical microscopy (Olympus MX51) after the samples were polished to mirror finish. All the

samples were cut and mounted along the YZ plane (Figure 2). To bring the samples to mirror, the optical microscopy samples were organized into similar parameter sets and orientation angles, then arranged from least to greatest thickness. The samples were then mounted in an acrylic molding mixture for a total of 27 individual pucks, 9 parameter sets in three different orientation with five individual samples per puck. The pucks were then ground and polished using the Allied High Tech MetPrep 3 Automatic Polisher using their recommended polishing procedure. The samples were then imaged on a high-resolution light microscope. The images were analyzed using ImageJ for porosity analysis. Additional samples with larger overall length and shorter overall height (Figure 3) were fabricated for the mechanical testing. For mechanical property evaluation, the samples were subjected to three-point bending in order to evaluate the ultimate strength. For the three-point bending test, a custom micro three-point bending fixture was designed, and the testing was carried out on an Instron 5569A universal testing system using 50N load cell. The test setup is shown in Figure 4.

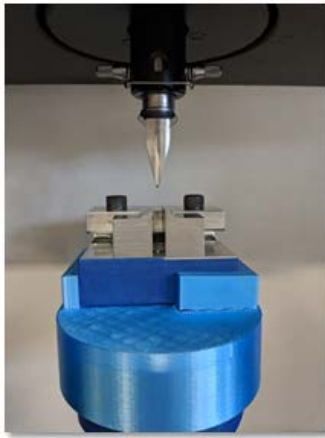


Figure 4. Three-point bending fixture setup with alignment tool and mount

Results and Discussion

The results for the porosity measurements of the optical microscopy samples, the ultimate shear stress from the three-point bending and the dimensional accuracy taken from the measured thickness of the specimens and compared to the design thickness, print orientation and processing parameters to check for significant correlations.

As shown in Figure 5, the dimensional accuracy exhibits significant dependency on both the design thickness and build orientation. It appears that the process reaches resolution limit with thicknesses smaller than 0.2mm. The dimensional variability of the samples also exhibit significant increasing trend as the design dimensions decreases. This could be readily explain in that for the fabrication of small-dimension features, the effect of surface sintering and melt-track trajectory fluctuation becomes more significant relative to the actual feature. Thin walls at higher print orientation angles also exhibit lower overall relative errors. This is probably attributed to the fact that the support structure is absent for lower orientation angle and that the relatively large melt pool resulted from the oblique cross section exhibits more significant gravity-induced distortion. This shows that for thin wall structures the use of support structure might still be beneficial or even necessary.

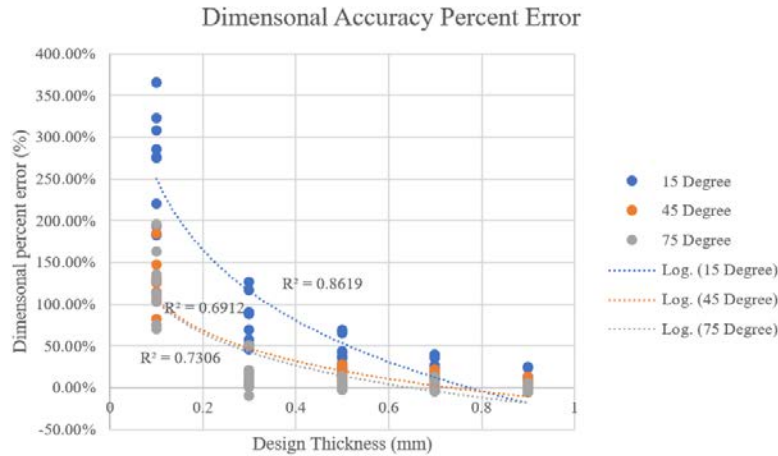
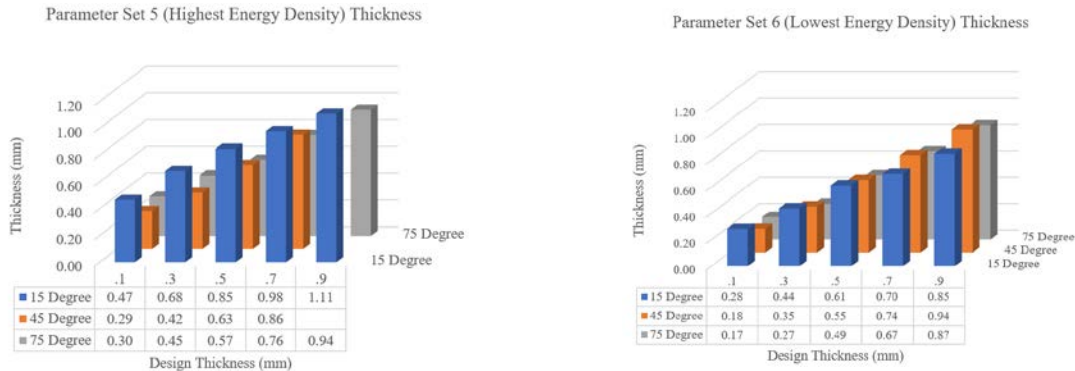


Figure 5. Dimensional accuracy relative percent error vs. design thickness and print orientation

Figure 6 compares the thickness characteristics of all the thin wall samples at the highest energy density level versus the lowest energy density level. There is no significant difference between the highest and lowest energy density in terms of the thickness of fabricated thin walls. Even though the high-energy density parameter set appears to result in slightly higher overall dimensions, when standard deviation was factored in the difference becomes insignificant. Therefore, within the range of values investigated in this study, process parameter settings do not appear to have significant impact on the dimensional accuracy of the thin wall structures.



a. Highest energy density level

b. Lowest energy density level

Figure 6. Thickness of walls at different energy density levels

Figure 7 shows groups samples from the same process parameter set and at three varying orientations. The thickness of the samples increases from lower left to upper right in each group. It is immediately clear that as the orientation angle increases the surface roughness also improves dramatically. This is expected to be also closely related to the absent of support structures and the consequent “mesoscale distortion” with the thin walls. Also for the lower-orientation thin walls the top section of the walls exhibit additional defects, which might be partly attributed to multiple factors. As the residual thermal stress accumulation over layers causes the thin wall to gradually exhibit more significant warping distortion, the “branch-out” type of shaping defect might occur at the top layer. Also, the thin wall feature could distort or fail due to the shear stress from the recoater blade as it passed over the part distributing more powder, as is obvious in the case of the 75° group (Figure 7), in which the 0.05mm sample failed to be built successfully. On

the other hand, there was a 100% build success rate for the 15° and 45° samples. The build failure was observed for all the 0.1mm 75° samples and was even observed for some 0.3mm samples. This, along with the branch-like defect, points to the limitations of the PBF-AM to manufacture parts with this type of thin geometry.

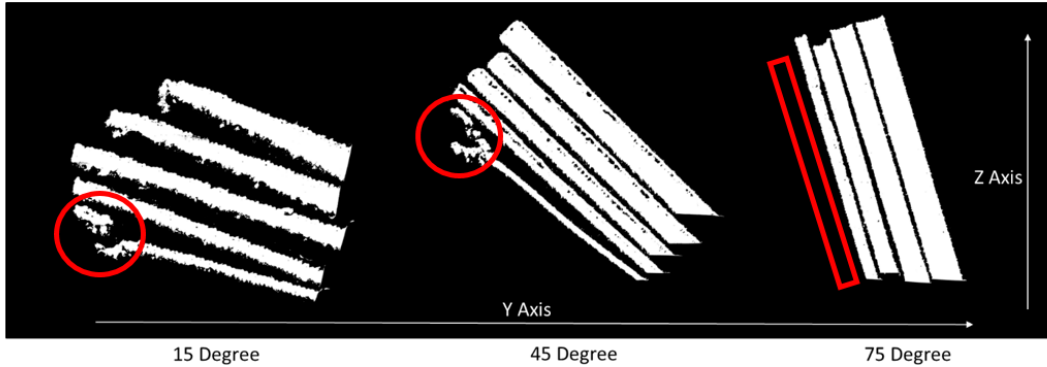


Figure 7. Optical microscopy images of thin wall samples in the three various print orientations

Figure 8 shows the three-point bending data. Most samples exhibit typical yielding and fracturing except the thinner 0.1 and 0.3 mm samples. For 0.1 mm samples, the samples exhibit bending yielding but no clear fracture, which might be attributed to the slipping and rotation of the samples relative to the two supports. Similar behavior can also be observed in the 0.3mm thick samples, while there was eventual fracture the samples would continue to yield past the maximum bending point and slowly tear instead of sudden shear. This can be observed in Figure 8 as the gradual decrease with a negative slope to a 0N load for sample 1-15-A-3 (parameter set 1, 15° print orientation, batch A, .3 mm thickness). For most other samples, as the thickness increases, a greater load could be supported by the thin wall prior to the catastrophic failure.

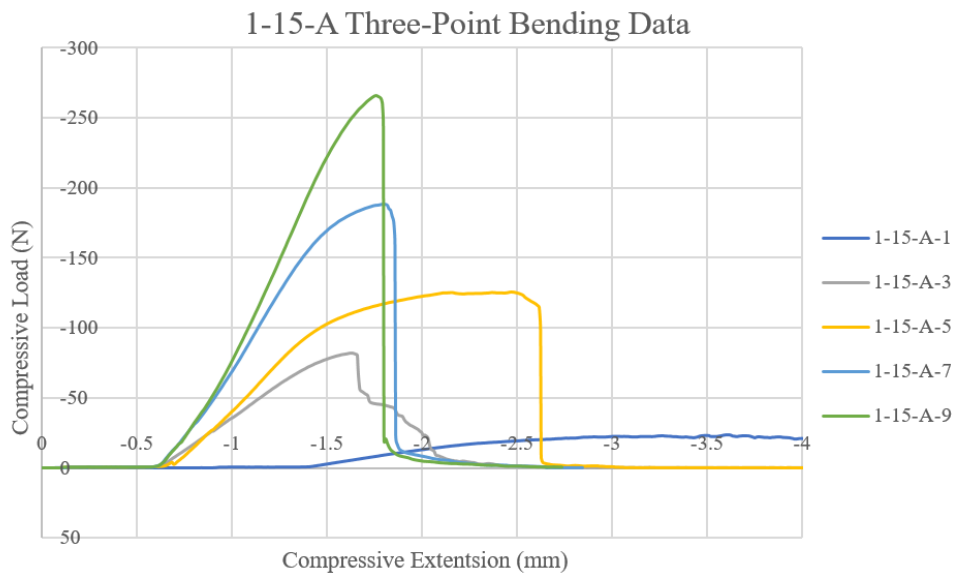


Figure 8: Typical three-point bending data received for samples across all print orientations and parameter sets

Figure 9 shows the ultimate shear stress for all of the samples. There is a slight positive trend that as the thickness of the sample increases so does the ultimate shear stress of the sample. On the other hand, the effect of orientation angle is more significant. The results show that as the print orientation angle increases the ultimate shear stress of the thin wall also increases.

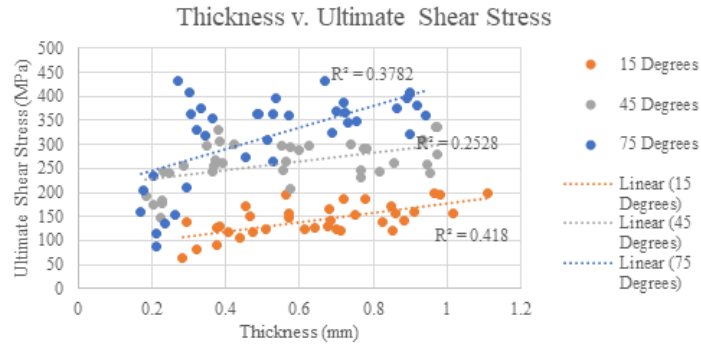


Figure 9: Ultimate shear stress plotted against measured thickness for all parameter sets across the three varying orientation angles

Figure 9 further illustrates the strength of the samples at different orientation angle under different process parameter set. There are two major conclusions to be drawn from this data. Firstly, it appears that as orientation angle increases the ultimate strength clusters of the samples becomes more scattered. This dispersion may mean that process parameter settings have more significant effect or that a higher orientation angle is detrimental to quality. Secondly, there does not appear to be a single parameter set that provides the highest ultimate shear strength across the varying sample thicknesses. Also, the effect of the process parameters appears inconsistent and relatively insignificant.

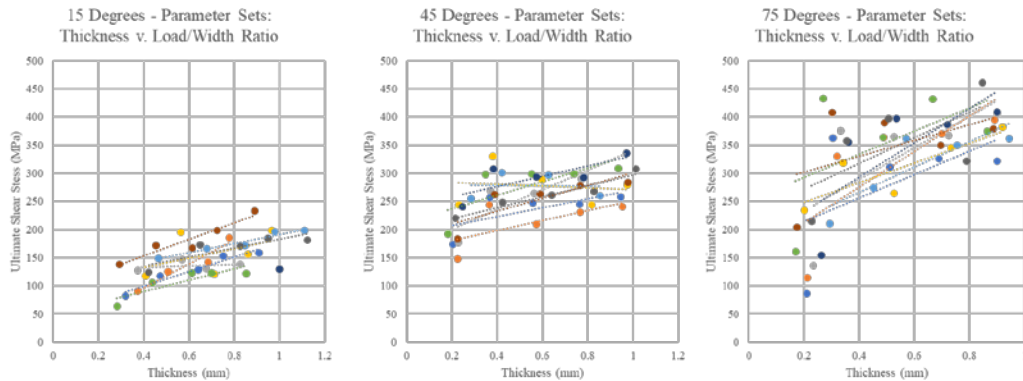


Figure 10. Ultimate shear stress plotted against measured thickness, divided up by orientation angle and grouped by parameter sets

Fig.11 shows the relative density values of the samples from the optical microscopy image-based analysis. From the results there is no apparent correlation between orientation angle or thickness and the porosities. As the orientation angle increases, there appears to be a general increase of porosity value variability, although the 45° group appears to exhibit considerably larger porosity variability compared to the other groups. Further studies are being carried out to investigate into this unusual observation.

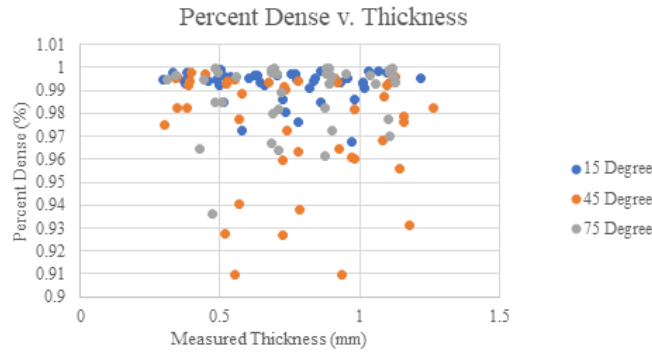


Figure 11. Percent density vs. the measured sample thickness

3. Conclusion

In the present study, thin wall samples manufactured on the EOSINT M 270 in Ti6Al4V were investigated for their quality and properties under varying geometry and process conditions. The results suggest that there is a positive correlation of the mechanical bending strength and dimensional accuracy against the orientation and design thickness of the thin wall. As the orientation angle or the thickness of the sample increases both the mechanical strength and the dimensional accuracy increases. No noticeable trend between the process parameter settings used in the study and any quality characteristics was observed. Also, no noticeable correlation was observed between the porosity and the geometrical or mechanical qualities of the parts. With the current system/material combination, the thin wall features with thickness below 0.3mm exhibits large quality variability and therefore should be avoided during the designs.

4. Acknowledgements

This research is partially supported by National Aeronautics and Space Administration (NASA) #NNM17AA10A. The authors would like to acknowledge the support from the University of Louisville Rapid Prototyping Center (RPC) and the help from Samuel Williams and Katherine Schneidau.

5. References

- [1] D. T. Queheillalt, H. N. G. Wadley. Hollow pyramidal lattice truss structures. *International Journal of Materials Research*. 102(2011), 4: 389-400.
- [2] M. F. Ashby. The properties of foams and lattices. *Philosophical Transactions of the Royal Society A*. 364(2006): 15-30.
- [3] L. Dong, V. Deshpande, H. Wadley. Mechanical response of Ti-6Al-4V octet-truss lattice structures. *International Journal of Solids and Structures*. 60-61(2015): 107-124.
- [4] T. R. Faisal, A. D. Rey, D. Pasini. A multiscale mechanical model for plant tissue stiffness. *Polymers*. 5(2013): 730-750.
- [5] A. Vigliotti, V. S. Deshpande, D. Pasini. Non linear constitutive models for lattice materials. *Journal of the Mechanics and Physics of Solids*. 64(2014): 44-60.
- [6] T. J. Lu, L. Valdevit, A. G. Evans. Active cooling by metallic sandwich structures with periodic cores. *Progress in Materials Science*. 50(2005): 789-815.

- [7] A.-J. Wang, R. S. Kumar, D. L. McDowell. Mechanical behavior of extruded prismatic cellular metals. *Mechanics of Advanced Materials and Structures*. 12(2005): 185-200.
- [8] Y.-H. Lee, B.-K. Lee, I. Jeon, K.-J. Kang. Wire-woven bulk Kagome truss cores. *Acta Materialia*. 55(2007): 6084-6094.
- [9] X. Y. Cheng, S. J. Li, L. E. Murr, Z. B. Zhang, Y. L. Hao, R. Yang, F. Medina, R. B. Wicker. Compression deformation behavior of Ti-6Al-4V alloy with cellular structures fabricated by electron beam melting. *Journal of the Mechanical Behavior of Biomedical Materials*. 16(2012): 153-162.
- [10] R. Gumruk, R. A. W. Mines. Compressive behaviour of stainless steel micro-lattice structures. *International Journal of Mechanical Sciences*. 68(2013): 125-139.
- [11] L. J. Gibson, M. F. Ashby. *Cellular Solids: Structure and Properties*. 2nd Edn. Cambridge University Press, 1997.
- [12] M. F. Ashby, A. G. Evans, N. A. Fleck, L. J. Gibson, J. W. Hutchinson, H. N. G. Wadley. *Metal Foams: A Design Guide*. Butterworth Heinemann, 2000.
- [13] P. Columbo. In Praise of Pores. *Science*. 332(2008): 381-383.
- [14] T. J. Lu. Heat transfer efficiency of metal honeycombs. *International Journal of Heat and Mass Transfer*. 42(1999): 2031-2040.
- [15] T. Kim, C. Y. Zhao, T. J. Lu, H. P. Hodson. Convective heat dissipation with lattice-frame materials. *Mechanics of Materials*. 36(2004): 767-780.
- [16] T. Kim, H. P. Hodson, T. J. Lu. Fluid-flow and endwall heat-transfer characteristic of an ultralight lattice-frame material. *International Journal of Heat and Mass Transfer*. 47(2004): 1129-1140.
- [17] K. F. Leong, C. M. Cheah, C. K. Chua. Solid freeform fabrication of three-dimensional scaffolds for engineering replacement tissues and organs. *Biomaterials*. 24(2003): 2363-2378.
- [18] D. A. Zopf, A. G. Mitsak, C. L. Flanagan, M. Wheeler, G. E. Green, S. J. Hollister. Computer aided-designed, 3-dimensionally printed porous tissue bioscaffolds for craniofacial soft tissue reconstruction. *American Academy of Otolaryngology- Head and Neck Surgery*. 152(2015), 1: 57-62.
- [19] W. T. Carter, D. J. Erno, D. H. Abbott, C. E. Bruck, G. H. Wilson, J. B. Wolfe, D. M. Finkhousen, A. Tepper, R. G. Stevens. The GE aircraft engine bracket challenge: an experiment in crowdsourcing for mechanical design concepts. *Proceedings of Solid Freeform Fabrication (SFF) Symposium*, Austin, TX, USA, 2014.
- [20] J. Schmelzle, E. V. Kline, C. J. Dickman, E. W. Reutzel, G. Jones, T. W. Simpson. Re(designing) for part consolidation: understanding the challenges of metal additive manufacturing. *ASME Journal of Mechanical Design*. 137(2015), 11: 111404.
- [21] 5 Things to know about Navy 3D printing. Navy Live Blog. Accessed Nov. 2016.